Physicochem. Probl. Miner. Process., 62(3), 2026, 224365

http://www.journalssystem.com/ppmp

Physicochemical Problems of Mineral Processing

ISSN 1643-1049

Phthalic acid-assisted rare earth leaching process from ionic rare earth ore: leaching behavior, kinetics, and complexation mechanism

Xiang Hong [1,3], Zhenyue Zhang [1], Xiangyi Deng [1,2], Xiaoliang Zhang [2], Hanjun Wu [3], Xiang Ma [1], Anfu Wang [1], Ruan Chi [1]

[1] School of Resource and Safety Engineering, Wuhan Institute of Technology, Wuhan 430073, China

[2] State Key Laboratory of Mineral Processing, BGRIMM Technology Group, Beijing 100160, China

[3] School of Chemistry and Environmental Engineering, Wuhan Institute of Technology, Wuhan 430073, China

Corresponding author: xiangyideng@126.com (Xiangyi Deng)

Abstract: The extraction of rare earth (RE) elements from ion-adsorption type RE ores relies on in-situ leaching technology. However, the leaching process faces technical challenges such as low leaching efficiency and limited recovery rates. In this study, $MgSO_4$ was used as the leaching agent, with phthalic acid (PA) introduced as a complexation-assisted additive to improve RE leaching efficiency. The addition of 0.15% PA increased the RE leaching efficiency by 12.4% compared to using $MgSO_4$ alone. Leaching kinetics results indicate that as PA concentration increases, the RE leaching process exhibits two-stage behavior, with the leaching process governed by the internal diffusion model. Spectrophotometric analysis revealed that the PA primarily forms 1:1 and 1:2 coordination compounds with RE^{3+}, thereby reducing the concentration of free RE^{3+} ions in solution. Quantum chemical calculations further revealed that the order of binding energies for the reactions between the four RE ions and hydrogen phthalate ion (PA^-) is: $Y^{3+} > Pr^{3+} > Nd^{3+} > La^{3+}$. The computational results are consistent with the electrostatic potential distribution of RE^{3+}, indicating that PA^- interacts more strongly with RE^{3+} ions possessing higher charge density. In aqueous solution, the carboxyl groups of PA release protons, and the resulting oxygen atoms serve as negatively charged sites that coordinate with electron-deficient RE^{3+} ions to form stable RE carboxylate complexes. This interaction promotes the desorption of RE ions from clay mineral surfaces, thereby enhancing RE leaching efficiency.

Keywords: rare earth, phthalic acid, leaching behaviour, leaching kinetics, complexation leaching

1. Introduction

China's rare earth (RE) resources exhibit a distinct geographical distribution, with light RE elements concentrated in the north and heavy RE elements predominant in the south. These resources are characterized by concentrated deposits, diverse types, and complex mineral associations. The northern region serves as the base for light RE production, with bastnaesite from the Bayan Obo mine in Baotou, Inner Mongolia, being the most significant source (Dutta et al., 2016; Tian et al., 2011). This deposit boasts the world's largest RE reserves and is China's primary production base for light RE elements (Traore et al., 2023). In contrast, medium and heavy RE resources are mainly concentrated in southern regions, particularly in Ganzhou, Longyan, and surrounding areas. Ionic RE ores are rich in medium and heavy rare earth elements and are hailed as "industrial vitamins" (Yu et al., 2019). Medium-to-heavy RE elements, owing to their unique optoelectronic and magnetic properties, enhance the wear resistance, thermal stability, and hydrogen storage capacity of materials when incorporated. They hold greater industrial value than light RE elements. These elements find extensive applications across multiple sectors, including military, aerospace, electronics, and advanced materials (Shuai et al., 2024; Li et al., 2025).

The raw ore grade of ionic RE ores is relatively low, typically containing only 0.05% to 0.20% RE oxides (Luo et al., 2022). RE elements are primarily adsorbed as ions onto clay minerals such as kaolinite, halloysite, and illite. When exposed to chemically more active electrolyte cations such as Na^+, K^+, and

DOI: 10.37190/ppmp/224365

NH_4^+, these adsorbed RE ions can be exchanged and released from the clay surfaces (Liu et al., 2023). The leaching process can thus be regarded as an ion-exchange reaction, wherein clay minerals function as an ion-exchange resin and a salt-based leaching solution acts as the mobile phase, displacing and recovering the RE ions.

For an extended period, $(NH_4)_2SO_4$ has been the primary leaching agent used in the leaching of ionic RE ores, resulting in the generation of large volumes of ammonia-nitrogen wastewater. This has led to elevated ammonia nitrogen levels in mining areas and the eutrophication of water bodies, posing serious threats to ecological safety (Yun et al., 2025). To mitigate the environmental pollution associated with the extensive application of $(NH_4)_2SO_4$, various improvement strategies-such as compound leaching using mixtures of ammonium, calcium, and magnesium salts-have been investigated (Feng et al., 2018). While these approaches have shown some success, the reduction in ammonium consumption remains limited, meaning they can only partially alleviate, rather than fundamentally resolve, ammonia-nitrogen pollution. To address the issue at its source, researchers have begun exploring novel leaching agents with zero ammonium content. $MgSO_4$ has emerged in recent years as a promising alternative (Han et al., 2025). It enables the leaching of RE elements without introducing ammonium and additionally helps replenish magnesium in magnesium-deficient soils. Guo et al. (2023) identified $MgSO_4$ as a suitable ammonium-free leaching agent for ionic RE ores and reported enhanced leaching performance. Similarly, Xiao et al. (2015) compared the leaching efficiencies of $(NH_4)_2SO_4$ and $MgSO_4$, and advocated for the replacement of $(NH_4)_2SO_4$ with $MgSO_4$ to prevent ammonia nitrogen pollution.

However, the leaching efficiency of RE elements remains low in the in-situ leaching process due to the high content of clay minerals (Wang et al., 2025). To tackle these challenges, researchers have turned to leaching aids to improve both RE extraction rates and solution permeability. Yang et al. (2024) investigated a composite leaching system comprising the surfactant polyethyleneimine (PEI) and $(NH_4)_2SO_4$. Their results demonstrated a reduction in leaching time by one-third, substantially lowering operational costs. In another study, Deng et al. (2024) applied hexadecyltrimethylammonium chloride (CTAC) to enhance the RE leaching process. CTAC was found to adsorb onto the surfaces of clay minerals, increasing the contact angle and raising the zeta potential, thereby improving permeability. Under optimized conditions, the RE leaching efficiency increased from 83.75% to 95.65%, and accelerated the leaching process. Wang et al. (2025) introduced itaconic acid as a leaching aid in a $MgSO_4$ system, where it formed soluble complexes with RE ions, enhanced the concentration gradient for ion diffusion, and increased the RE leaching efficiency by 9.34%. Similarly, Lai et al. (2018) employed a composite leaching agent of $MgSO_4$ and ascorbic acid, leveraging the coordinating and reducing properties of ascorbic acid to extract rare earth elements from both the ion-exchange phase and the colloidal phase.

In summary, research on RE leaching aids has primarily focused on the impact of leaching agents on the surface properties of clay minerals and the RE extraction process. However, there are few reports on the interactions between leaching agents and RE^{3+} ions in solution, as well as their effects on ion exchange. RE elements have a special case of electron orbital filling with strong coordination ability (Gao et al., 2023). For RE elements, the 5d orbitals are typically unoccupied in the ground state with higher in energy and more spatially extended compared with 4f orbitals. In the presence of strong-field ligands, electrons may be promoted from the 4f or 6s orbitals into 5d orbitals that can engage in covalent bonding with the ligand. The organic oxygen-containing groups in organic acids-such as C-O, P-O, and S-O can complex with RE^{3+} to form metal complexes, which also assists RE leaching from ionic RE ores (Wu et al., 2023; Zheng et al., 2018).

The above research provides important data and theoretical support for ionic RE ores mining. Stronger complexation between the solvent and RE ions in solution facilitates the desorption of RE elements from clay minerals. As a green, efficient, and highly selective auxiliary leaching agent for rare earth elements, phthalic acid offers remarkable environmental friendliness-being biodegradable and avoiding ammonia-nitrogen pollution-while exhibiting selective complexation capability toward rare earth ions over coexisting impurity cations (e.g., Al^{3+}, Ca^{2+}, Mg^{2+}, Fe^{3+}) in the ore. This study evaluates the benzene-ring-containing dibasic carboxylic acid as a novel leaching aid. The effects of individual operational parameters on RE leaching were investigated. Kinetic models for leaching in the presence of this aid were established. The mechanism by which complexation enhances leaching of RE bound as magnesium salts was elucidated.

2. Experimental

2.1. Materials

PA, sulfosalicylic acid, ascorbic acid, hexamethylenetetramine, zinc standard solution, $MgSO_4$, and ethylenediaminetetraacetic acid reagent were from Sinopharm Chemical Reagent Co. Ltd., and RE chlorides (lanthanum chloride, cerium chloride, neodymium chloride, and yttrium chloride) were purchased from Aladdin. All the agents in the experiment were analytically pure.

2.2. Ore sample

The ore samples were from Jiangxi Province, China. Samples were dried to constant weight. The main chemical composition of ionic rare earth ore was determined by X-ray fluorescence (XRF; Malvern Panalytical, Axios, Netherlands). As shown in Table 1, the major ore components were SiO_2 (55.4%) and Al_2O_3 (37.9%). Specifically, the total rare-earth element content was 0.0687% as determined by inductively coupled plasma mass spectrometry (ICP-MS; Shimadzu, model 2030, Japan) in accordance with national standard methods (GB/T 40798-2021). The distribution of ion-exchangeable RE elements was determined by ICP-MS. Specifically, 2.00 g of the dried ore sample was mixed with 20 mL of 50.00 g/L $(NH_4)_2SO_4$ solution. The mixture was stirred at 300 rpm for 2.0 h to ensure the complete exchange of adsorbed RE^{3+} ions by NH_4^+. After reaching equilibrium, the suspension was filtered through a 0.45 μm membrane filter, and the RE concentration in the filtrate was determined by ICP-MS. Table 2 shows that the exchangeable RE elements are dominated by yttrium (Y_2O_3; 28.72%), neodymium (Nd_2O_3; 22.34%), and lanthanum (La_2O_3; 20.44%). Additionally, minerals in the raw ore sample were identified by X-ray diffraction (Bruker Corporation, Advanced D8, Germany). Measurements were performed using Cu Kα radiation (λ = 1.5418 Å) with a nickel filter, a 2θ scan range of 5°-85°, and a scan rate of 5° min^{-1}. The XRD pattern is shown in Fig. 1. The diffraction peak at 2θ ≈ 27° is formed by the superposition of characteristic peaks from Albite, Muscovite, and Quartz, resulting in increased peak intensity and a slight shift in the diffraction peak.The major mineral phases are Kaolinite (PDF#14-0164), Quartz (PDF#79-1906), and Albite (PDF#83-1610), while the minor mineral phases are Muscovite (PDF#07-0042) and Halloysite (PDF#29-1489).

Table 1. Main chemical composition of ionic RE ore(wt.%)

Element	REO	SiO_2	Al_2O_3	Fe_2O_3	K_2O	Na_2O	MnO	Rb_2O
Content	0.0687	55.4	37.9	1.46	3.73	0.933	0.107	0.137

Table 2. Distribution of ion-exchangeable RE (wt.%)

Element	Y_2O_3	Nd_2O_3	La_2O_3	Pr_2O_3	Sm_2O_3	Gd_2O_3	Tb_2O_3	Er_2O_3
Content	28.72	22.34	20.44	6.85	5.07	4.72	4.54	2.31

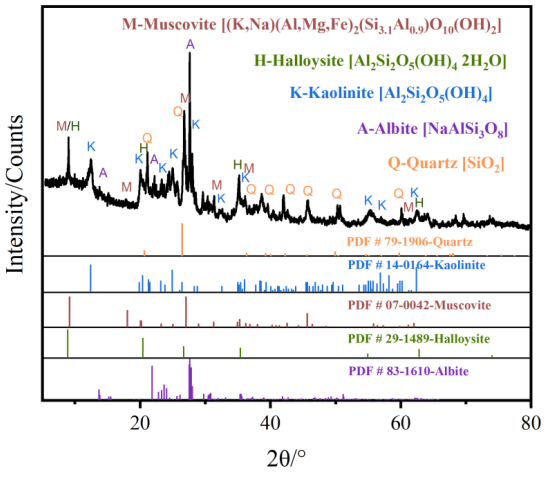

Fig. 1. XRD pattern of ionic rare earth ore

2.3. Experimental procedures

2.3.1. Leaching experiment

The column leaching process for RE ores is schematically illustrated in Fig. 2. A solution of 0.20 mol/L $MgSO_4$ was employed as the primary leaching agent, with different PA concentrations added as a leaching aid. Fifty grams of dried ionic RE ores sample was weighed and evenly packed into a custom chromatography column (internal diameter 30 mm) with an ore bed height of 7.7 cm. The leachate was continuously supplied using a constant-flow pump (Baoding Lange Constant Flow Pump Co., Ltd., BT100-2J, China) at a constant flow rate to maintain a fixed liquid level and a stable hydrodynamic gradient throughout the leaching process. Effluent samples were collected from the bottom of the column using a beaker. Leachate was collected until no further leachate was discharged. The samples were analyzed for RE content by EDTA complexometric titration.

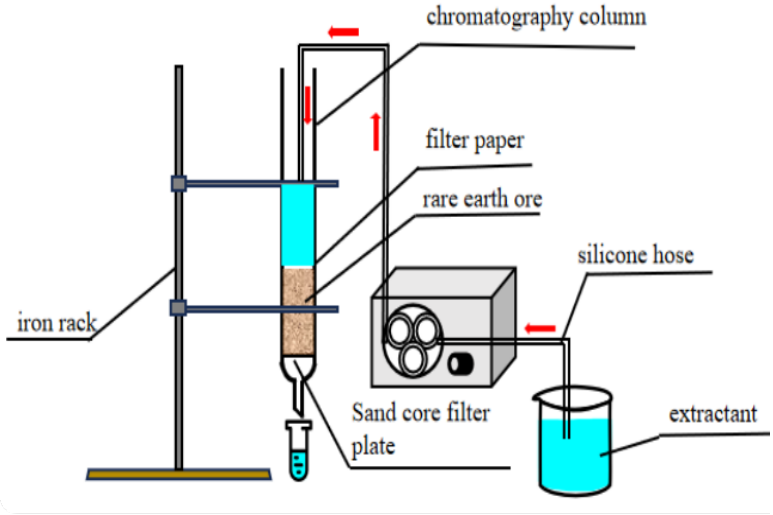

Fig. 2. Schematic diagram of RE leaching device

2.3.2. Determination of RE content in the leachate

The RE content in the leachate was determined by EDTA titration based on the 1:1 stoichiometric complexation between RE^{3+} and EDTA (Yan et al., 2018; Yang et al., 2019). The determination principle involves the following steps: First, Impurity ions such as Fe^{3+} and Al^{3+} were first masked using ascorbic acid and sulfosalicylic acid to prevent interference. The solution pH was then adjusted to 5.5 (0.1 mol/L NaOH and 0.1 mol/L H_2SO_4) using hexamethylenetetramine serving as a buffer. At this pH, dimethylphenol orange was added as the indicator, which can coordinate with RE^{3+} to form a purplish-red complex. As the standard EDTA solution is added, it reacts with RE^{3+} ions to form a more stable complex, releasing the free indicator and resulting in a distinct visual color change from purplish-red to bright yellow. The RE content was then calculated using Eq. 1. The RE leaching efficiency was calculated using Eq. 2.

$$C_{REO} = \frac{C_{EDTA} \times V_{EDTA}}{2V} \times M_{REO} \quad (1)$$

$$a = \frac{m_1}{m} \times 100\% \quad (2)$$

where C_{REO} indicates the concentration of RE, g/L; V_{EDTA} is the average volume of EDTA consumed in several parallel titration tests, mL; V is the volume of the solution measured, mL; and M_{REO} is the average relative molecular mass of RE oxides, g/mol. a is the leaching efficiency of RE; m_1 is leaching RE mass; m is ion-exchange RE mass.

2.3.3. Determination of complex composition

In aqueous solution, PA forms complexes with RE ions, facilitating their desorption. The RE complexes composition can be determined using the molar ratio method using a UV-Vis spectrophotometer (Shimadzu Corporation, UV-2450, Japan) (Mabrouk et al., 2018). To determine the stoichiometry of the

complexation reaction M + nY→MY_n (M and Y denote the metal cation and the ligand, respectively), the ligand concentration was varied. The absorbance of each solution was measured at the complex's absorption maximum, and absorbance was plotted versus the molar ratio C_Y/C_M. Absorbance increased linearly with the C_Y/C_M until the complex's stoichiometric ratio was reached. Further increases in C_Y/C_M produced a plateau, indicating that the absorbance originated exclusively from the formed complex (Hoshino et al., 2011). The stoichiometry of the complex was determined by extrapolating the linear portion of the curve.

2.3.4. Quantum chemical calculations

Based on density functional theory (DFT), a complexation reaction model between hydrogen phthalate ion (PA^-) and RE^{3+} was established using the DMol³ software in Materials Studio. On this basis, the electrostatic potential energy and reaction binding energy between four RE^{3+} and PA^- were calculated. In the density functional theory calculations, the generalized gradient approximation GGA-BLYP model was employed to optimize the exchange correlation function for structural refinement. Following optimization of the stable configurations, high-precision single-point energy calculations were performed to determine the component energies. The coordination reaction binding energies were calculated using the following formula (Liu et al., 2025).

$$E_{PA-RE} = E_{total} - E_{PA} - E_{RE} \quad (3)$$

where $E_{PA\text{-}RE}$ represents the binding energy; E_{total} represents the energy after the complexation of PA and RE; and E_{PA} and E_{RE} represent the energies of the two monomers, respectively.

3. Results and discussion

3.1. RE leaching behavior in PA-$MgSO_4$ system

3.1.1. Effect of $MgSO_4$ and PA concentration on the leaching efficiency of RE

The effect of PA concentrati on the leaching efficiency of RE is shown in Fig. 3. The results indicate that the RE leaching efficiency increased with rising $MgSO_4$ concentration in the absence of PA. At 0.20 mol/L $MgSO_4$, the leaching efficiency reached a maximum. Further increases produced negligible change. Fig. 3(B) shows that adding PA at appropriate concentrations significantly enhanced the leaching efficiency of RE. Compared with the $MgSO_4$-only system, the presence of PA increased RE leaching efficiency to varying extents. This improvement is attributed to the carboxyl groups in PA, which can form stable complexes with RE^{3+} ions, thereby facilitating their release and enhancing overall leaching efficiency (Zhao et al., 2025). However, as the concentration of PA increased, the leaching efficiency of RE began to decline. The optimal PA concentration was determined to be 0.15%, at which point the leaching efficiency reached 96.81%, representing a 12.4% improvement compared to the system without PA.

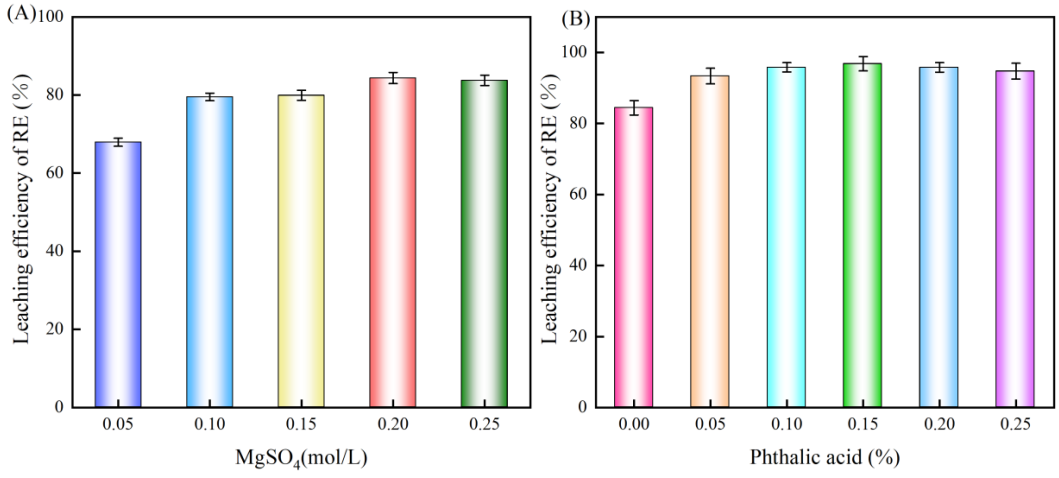

Fig. 3. Effect of $MgSO_4$ concentration (A) and PA concentration (at 0.20 mol/L $MgSO_4$) on the leaching efficiency of RE (B)

3.1.2. Effect of pH on RE leaching process

Fig. 4(A) illustrates the effect of initial leaching solution pH on RE leaching efficiency under the conditions of 0.20 mol/L $MgSO_4$ and 0.15% PA. At the same pH, PA can significantly increase the RE leaching efficiency. Leaching efficiency reached 94.46% at an initial pH of 2.0 but decreased to 90.24% at pH 6.0. As an exchange cation, H^+ can directly undergo ion exchange with RE ions adsorbed on the surface of clay minerals, displacing the RE ions from their adsorption sites. Furthermore, H^+ can protonate -OH on the mineral surface, altering the surface charge properties of the clay minerals and weakening their electrostatic adsorption capacity for RE^{3+} ions. The combined effect of these two mechanisms promotes the release of RE ions from the mineral surface into the solution.

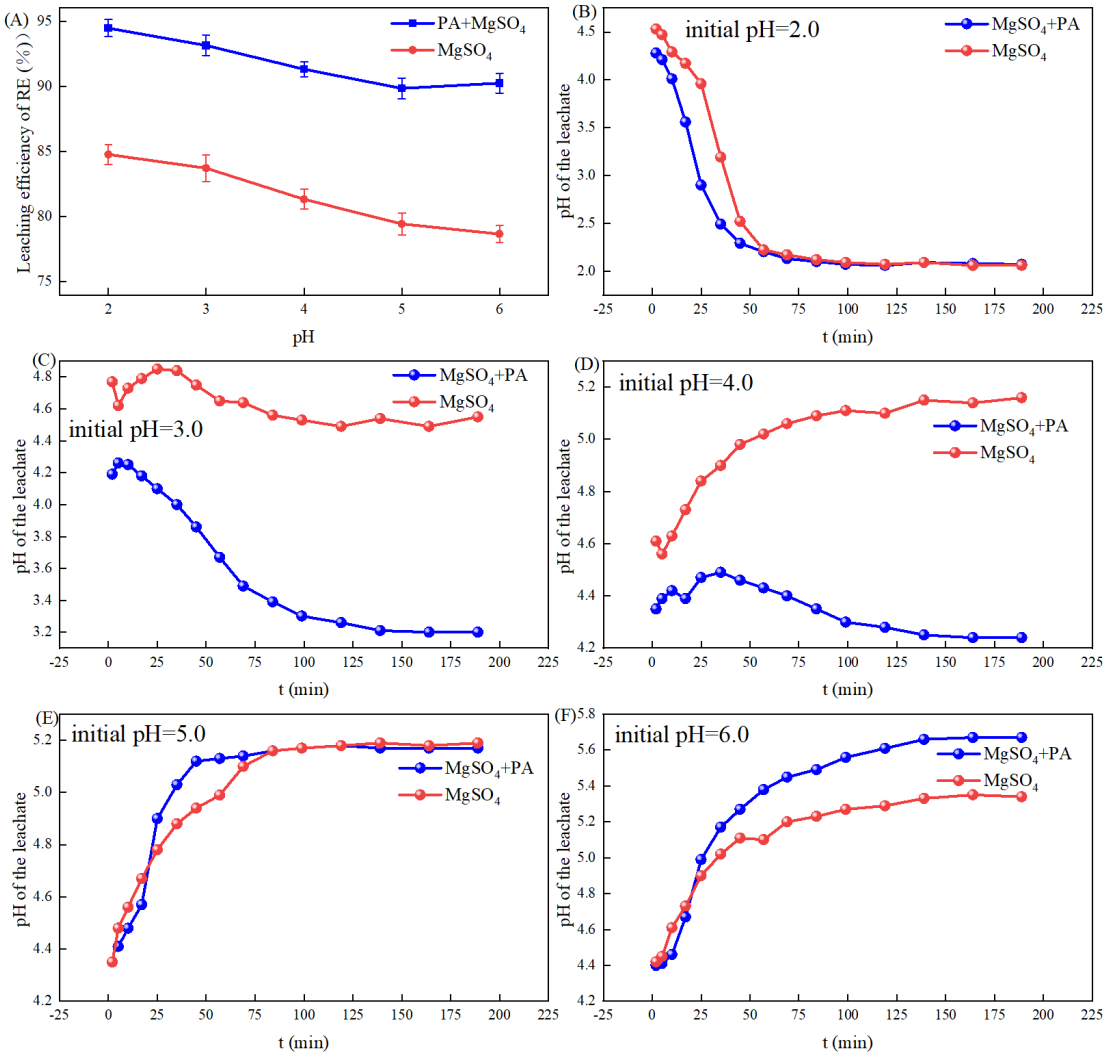

Fig. 4. Effect of initial pH of leaching agent solution on the leaching efficiency of RE(A) and the pH of leachate over time at initial pH 2.0(B), 3.0(C), 4.0(D), 5.0(E), and 6.0(F), respectively

Fig. 4 (B)-(F) shows the pH of leachate over time at different initial pH ranging from 2.0 to 6.0. As illustrated in Fig. 4(B), when the pH is exceedingly low (pH=2.0), H^+ occupy the exchangeable sites on the surfaces of clay minerals, resulting in a higher leachate pH compared to the initial pH in both $MgSO_4$ and $MgSO_4$-PA system solutions. As leaching time increases, the pH of the leachate gradually decreases. When the initial pH is raised to 3.0 (Fig. 4(C)), H^+ in the $MgSO_4$ system is initially consumed, leading to an increase in pH. Subsequently, an excess of H^+ develops, resulting in a gradual rise in system pH. In the $MgSO_4$-PA system, anion of PA can bind with H^+ ions. As the reaction progresses, H^+ bound to anions are released, causing the pH to initially increase and then decrease. The pH of the leaching solution is significantly lower than that of the $MgSO_4$ solution. When the initial pH rises to 4.0 (Fig. 4(D)), H^+ in the $MgSO_4$ system are continuously consumed, indicating a gradual increasing trend. In

the $MgSO_4$-PA system, the pH evolution of the leachate resembles that observed at an initial pH of 3.0, but with a substantially reduced amplitude. When the initial pH is further increased to 5.0 (Fig. 4(E)), the H^+ in the solution decreases, and proton exchange between the $MgSO_4$ and $MgSO_4$-PA system solutions and the surface ions of clay minerals reaches equilibrium, stabilizing the leachate pH at approximately 5.18. When the pH is elevated to 6.0 (Fig. 4(F)), the leachate pH exceeds that of the $MgSO_4$ system due to the affinity of PA anions for protons.

3.2 Effect of PA concentration on RE leaching kinetics

The leaching of ionic RE ores is fundamentally an ion-exchange reaction, representing a typical liquid-solid heterogeneous phase process. The leaching of RE elements is reversible and can be controlled by one of four kinetic mechanisms (Parhi and Park, 2013; Wang et al., 2025). The corresponding kinetic equations for the leaching process are as follows:

- Chemical reaction control model:

$$1-(1-a)^{1/3}=k_1t \tag{4}$$

- External diffusion control model:

$$1-(1-a)^{1/3}=k_2t \tag{5}$$

- Internal diffusion control model:

$$1-\frac{2a}{3}-(1-a)^{2/3}=k_3t \tag{6}$$

- Hybrid diffusion control model:

$$1-(1-a)^{1/3}=\frac{k_1k_2}{k_1+k_2}\times\frac{C_0M}{r_0\rho}t \tag{7}$$

where a is the RE leaching efficiency, k is the reaction rate constant at different stages, C_0 is the initial concentration, r_0 is the particle size of RE, ρ is the molar density of RE, and M is the mass of RE.

PA concentration was varied to investigate its effect on the kinetics of RE leaching. In this experiment, different PA concentrations were combined with $MgSO_4$ to function as composite leaching agents. As presented in Fig. 5(A), RE leaching efficiency increased rapidly with time and gradually plateaued after approximately 150 min, reaching its maximum value and then maintaining equilibrium. As the concentration of PA increased, the leaching process accelerated continuously. When the PA concentration reached 0.15%, the equilibrium time was reduced by 50 min compared to the system without PA. Within a specific concentration range, the leaching efficiency of RE increased with rising concentrations of PA due to its ability to form stable complexes with RE^{3+} ions. This complexation facilitates the continuous desorption of RE^{3+} ions from the surfaces of clay minerals. However, when the PA concentration exceeded 0.15%, the leaching efficiency decreased, likely due to increased solution viscosity, which reduces penetration efficiency and prolongs the time required to reach leaching equilibrium (Liu et al., 2025).

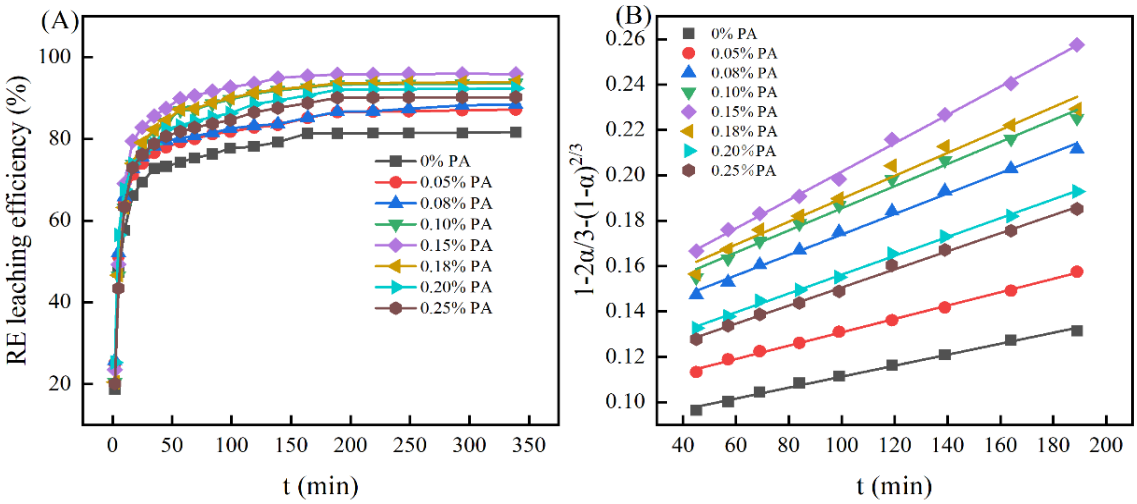

Fig. 5. Effect of PA concentration on RE leaching efficiency (A) and fitting diagram using the internal diffusion control model (B)

It is worth noting that the initial stage of leaching exhibited an extremely rapid RE release. This "initial burst" is attributed to the instantaneous ion exchange of RE^{3+} ions adsorbed on the outer surfaces of clay particles and the external film diffusion process. As the leaching progresses, the reaction interface moves into the interior of the mineral pores, where internal diffusion becomes the rate-limiting step. Therefore, the kinetic fitting focuses on this dominant stage to accurately reflect the complexation-assisted diffusion mechanism facilitated by PA. The data presented in Fig. 5(A) were fitted to four kinetic control models. Among these models, the equation $1 - 2a/3 - (1 - a)^{2/3}$ exhibited the best linear correlation with time (t), indicating that the RE leaching process was governed by internal diffusion. As shown in Fig. 5(B), the internal diffusion kinetic model demonstrated strong linearity, with correlation coefficients (R^2) exceeding 0.97 in all cases. This indicates that the leaching process of RE ore using PA as leaching aid is governed by internal diffusion control model (Chen et al., 2022). The k values at various PA concentrations were derived from the linear fitting results. The fitting results of the internal diffusion control model are presented in Table 4.

Table 4. Fitting results of the internal diffusion control model

C_{PA} (wt.%)	0	0.05	0.08	0.10	0.15	0.18	0.20	0.25
k/min^{-1}(10^{-4})	2.42	2.94	4.51	4.87	6.24	5.04	4.41	3.98
R^2	0.993	0.993	0.994	0.993	0.993	0.978	0.993	0.993

Additionally, the internal diffusion kinetic equation can also be expressed in a concentration-dependent form as follows (Li et al., 2013; Feng et al., 2018):

$$1 - \frac{2a}{3} - (1 - a)^{\frac{2}{3}} = (k_0 + k_{RE}C_0^n)t \tag{8}$$

The following relationship can be derived by $\ln(k - k_0) = nlnC_0 + lnk_{RE}$ combining the internal diffusion kinetic equation:

$$k = k_0 + k_{RE}C_0^n \tag{9}$$

$$\ln(k - k_0) = nlnC_0 + lnk_{RE} \tag{10}$$

where k_0 and k_{RE} are the apparent rate constants for RE leaching using $MgSO_4$ and $MgSO_4$ solution containing PA as leaching agents, respectively; n is the empirical reaction order of rare earth; C_0 is the concentration of PA in the leaching solution, mol/L; a is the leaching rate of RE; and t is the leaching time, min.

Based on the k values presented in Table 4, $ln(k\text{-}k_0)$ was plotted against lnC_0 using Eq. 10, and the results are displayed in Fig. 6. The fitted internal diffusion kinetic equations demonstrate a two-stage relationship as PA concentration increases.

As shown in Fig. 6(A), when the PA concentration ranges from 0 to 0.15%, the empirical reaction order (n) for RE leaching is 0.6896. The apparent rate constant k_{RE} is 0.016 obtained from linear fitting. Accordingly, the kinetic equation for RE leaching in the presence of PA at concentrations between 0 and 0.15% can be expressed as follows:

$$1 - \frac{2a}{3} - (1 - a)^{\frac{2}{3}} = 0.000242 + 0.016c_0^{0.6896})t \tag{11}$$

As shown in Fig. 6(B), when the PA concentration exceeds 0.15%, the empirical reaction order (n) for RE is -0.8793, and the corresponding apparent rate constant k_{RE} is 0.00005. Therefore, the kinetic equation for RE leaching at PA concentrations greater than 0.15% is:

$$1 - \frac{2a}{3} - (1 - a)^{\frac{2}{3}} = 0.000242 + 1.0 \times 10^{-5}c_0^{-0.8793})t \tag{12}$$

The negative empirical reaction order reflects the inhibitory effect of reactant concentration on leaching efficiency. Specifically, a negative reaction order indicates that, for PA concentrations exceeding 0.15%, the leaching efficiency of RE is reduced. The magnitude of the empirical reaction order reflects the extent to which PA concentration influences the reaction rate. These findings suggest that PA enhances RE leaching efficiency within a specific concentration range, but excessive PA concentrations inhibit the process (Wang et al., 2025). This further confirms that PA, as a leaching aid, significantly impacts the leaching behavior of ionic RE ores. When the PA concentration is low, the

solution viscosity is low, and mass transfer resistance in the system is minimal. This allows the ligand to diffuse fully and interact effectively with the rare earth ions, resulting in good leaching performance. However, when the PA concentration is too high, the solution viscosity increases significantly, the rate of ion diffusion decreases, and mass transfer resistance rises. This hinders the migration and contact of the ligand with the mineral particle surfaces, thereby inhibiting the leaching reaction process and ultimately leading to a decrease in rare earth leaching efficiency (Deng et al., 2024).

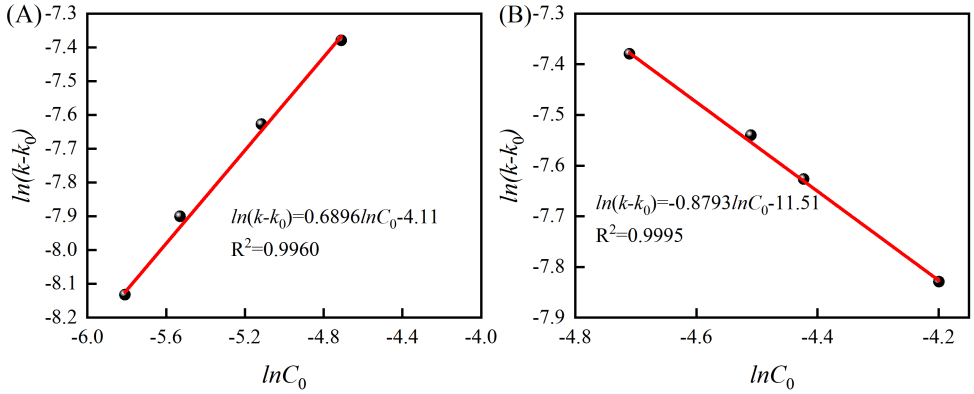

Fig. 6. The diagram of the relationship between $ln(k-k_0)$ and lnC_0

3.3. Enhanced leaching mechanism of PA with RE^{3+} complexation

3.3.1. Species distribution of PA

PA is a dibasic carboxylic acid that undergoes stepwise ionization in aqueous solution (Chang et al., 2022). Its ionization reactions are as follows:

$$C_8H_6O_{4(aq)} \rightarrow C_8H_5O_{4(aq)}^- + H^+{}_{(aq)} \quad K_1 = 1.12 \times 10^{-3} \tag{13}$$

$$C_8H_5O_{4(aq)}^- \rightarrow C_8H_4O_{4(aq)}^{2-} + H^+{}_{(aq)} \quad K_2 = 3.91 \times 10^{-6} \tag{14}$$

where K_1 and K_2 are the dissociation constants of PA.

$$K_1 = \frac{[C_8H_5O_4^-]\times[H^+]}{[C_8H_6O_4]} \tag{15}$$

$$K_2 = \frac{[C_8H_5O_4^{2-}]\times[H^+]}{[C_8H_5O_4^-]} \tag{16}$$

$$[PA]_r = [C_8H_6O_4] + [C_8H_5O_4^-] + [C_8H_5O_4^{2-}] \tag{17}$$

The percentage composition of each component in the PA solution is expressed as follows: θ_0 represents $C_8H_4O_4^{2-}$, θ_1 represents $C_8H_5O_4^-$, and θ_2 represents $C_8H_6O_4$.

$$\theta_0 = \frac{[C_8H_4O_4^{2-}]}{[PA]_r} = \frac{K_1K_2}{[H^+]^2+K_1[H^+]+K_1K_2} \tag{18}$$

$$\theta_1 = \frac{[C_8H_5O_4^-]}{[PA]_r} = \frac{K_1[H^+]}{[H^+]^2+K_1[H^+]+K_1K_2} \tag{19}$$

$$\theta_2 = \frac{[C_8H_6O_4]}{[PA]_r} = \frac{[H^+]^2}{[H^+]^2+K_1[H^+]+K_1K_2} \tag{20}$$

The distribution pattern of the species composition of PA, as shown in Fig. 7, is derived from Eqs. (18) to (20). At pH = 8.0, PA predominantly exists as $C_8H_4O_4^{2-}$, accounting for approximately 98% of the species present. As the pH decreases to 4.0, the proportion of $C_8H_4O_4^{2-}$ decreases significantly, while $C_8H_5O_4^-$ becomes the dominant form, comprising more than 85% of the total PA. At pH = 3.0, PA primarily exists in two forms, $C_8H_6O_4$ and $C_8H_5O_4^-$, which are present in nearly equal proportions, each accounting for approximately half of the total content. Under highly acidic conditions (pH < 1), PA exists almost entirely as $C_8H_6O_4$.

3.3.2. Species distribution of PA with RE^{3+} (La^{3+}, Pr^{3+}, Y^{3+}, Nd^{3+})

Visual MINTEQ calculations were performed to determine complexes species distribution of PA with RE^{3+} in the leachate. The complexes species distribution of PA with La^{3+}, Pr^{3+}, Y^{3+}, Nd^{3+} are shown in

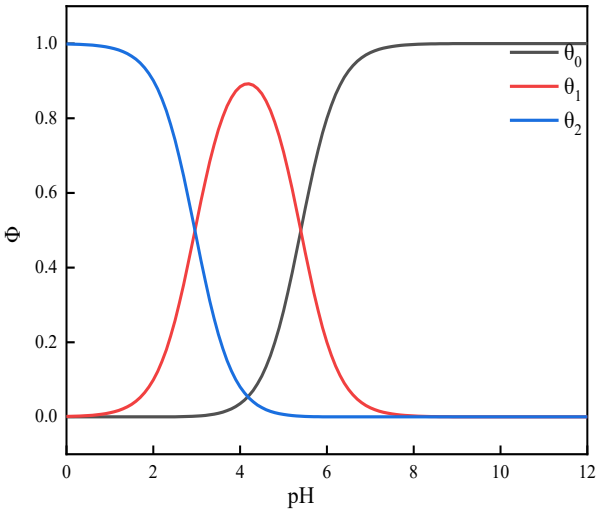

Fig. 7. Distribution pattern of species composition of PA

Fig. 8 (A), Fig. 8(B), Fig.8 (C) and Fig.8 (D), respectively. The species in each system undergo a transformation with increasing pH, progressing from free RE^{3+} ions to complexes with PA, and finally to hydroxide precipitates. When the pH is below 4, rare earth elements in the leachate primarily exist as metal ions (La^{3+}, Pr^{3+}, Y^{3+}, Nd^{3+}), while PA mainly exists as molecules and PA^-. When the pH is between 4 and 7, which corresponds to the favorable pH range for PA to function as a complexing agent, RE^{3+} ions form complexes with PA^- (La-PA, Pr-PA, Y-PA, Nd-PA), with RE-PA complexes becoming the dominant species. The complexation ratio of the four RE ions with PA exceeds 92%, while the proportion of free ions and ligands decreases significantly. At pH values above 7, the complexes gradually dissociate, and RE^{3+} ions subsequently react with OH^- to form RE hydroxide precipitates ($La(OH)_3$(s), $Pr(OH)_3$ (s), $Y(OH)_3$ (s), and $Nd(OH)_3$(s)). Particularly, La^{3+} and Pr^{3+} precipitate at higher pH values than Y^{3+} and Nd^{3+}.

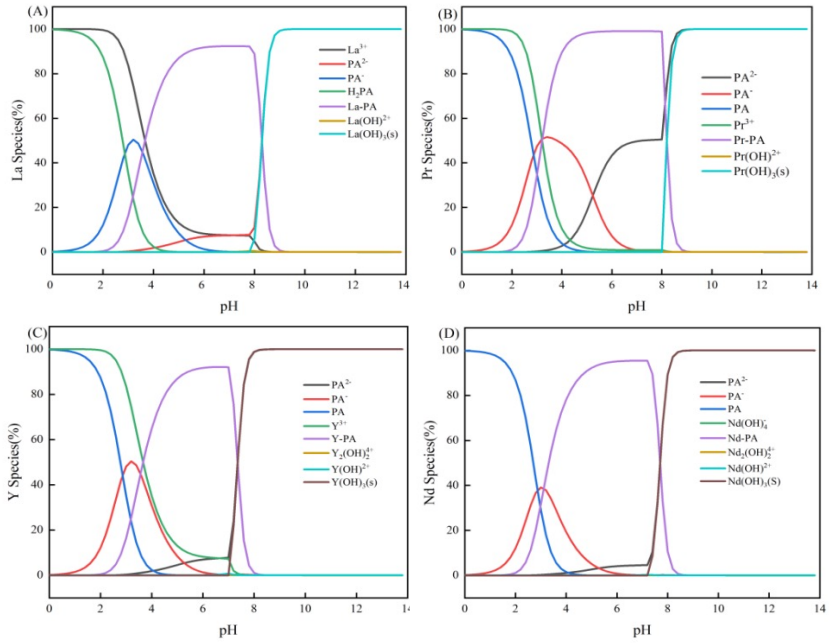

Fig. 8. Complexes species distribution of PA with La^{3+}(A), Pr^{3+}(B), Y^{3+}(C), Nd^{3+}(D), respectively

3.3.3. Uv-vis absorption characteristics of PA and RE^{3+} ions

The UV-Vis absorption spectra of $LaCl_3$, $PrCl_3$, YCl_3 and $NdCl_3$ solutions are shown in Fig. 9(A)-(D), respectively. The absorbance characteristics of RE^{3+} ions under ultraviolet wavelength scanning exhibit

significant variations. The absorption observed in individual RE chloride solutions is primarily attributed to the f-f electronic transitions of RE elements within their hydrated ionic forms, which are closely related to the number of unpaired 4f electrons (Guo et al., 2016). Lanthanum (La^{3+}) with an electron configuration of $4f^0$, is more stable due to the absence of 4f electrons, there is only one weak absorption peak at approximately 300 nm. Pr^{3+} exhibits a relatively strong absorption peak around 300 nm in the UV-visible region. Neodymium (Nd^{3+}, $4f^3$) and yttrium (Y^{3+}) display absorption in both the ultraviolet and visible regions. Additionally, the spectral bands are relatively narrow because the 4f orbitals are shielded by outer orbitals, making them less affected by solvent polarity or ligand field effects. Notably, absorption peaks were observed for all four RE^{3+} ions near 300 nm, whereas no common peaks were detected at other wavelengths.

The UV-Vis absorption spectrum of the PA solution is shown in Fig. 9(B). PA exhibits a strong absorption peak at 295 nm. As an organic carboxylic acid, PA contains a conjugated system, and the absorption at approximately 295 nm corresponds to a $\pi \rightarrow \pi^*$ electronic transition. This transition involves the excitation of π electrons from bonding orbitals to antibonding orbitals. The energy required for this transition corresponds to the photon energy at 295 nm, resulting in the observed strong absorption peak (Devangad et al., 2018).

The absorbance curves at different PA concentrations were shown in Fig. 9(C). As the PA concentration increased, the absorbance showed a corresponding upward trend. However, when the PA concentration reached 0.40%, the absorbance plateaued, remaining nearly constant at approximately 1.9, regardless of further increases in concentration.

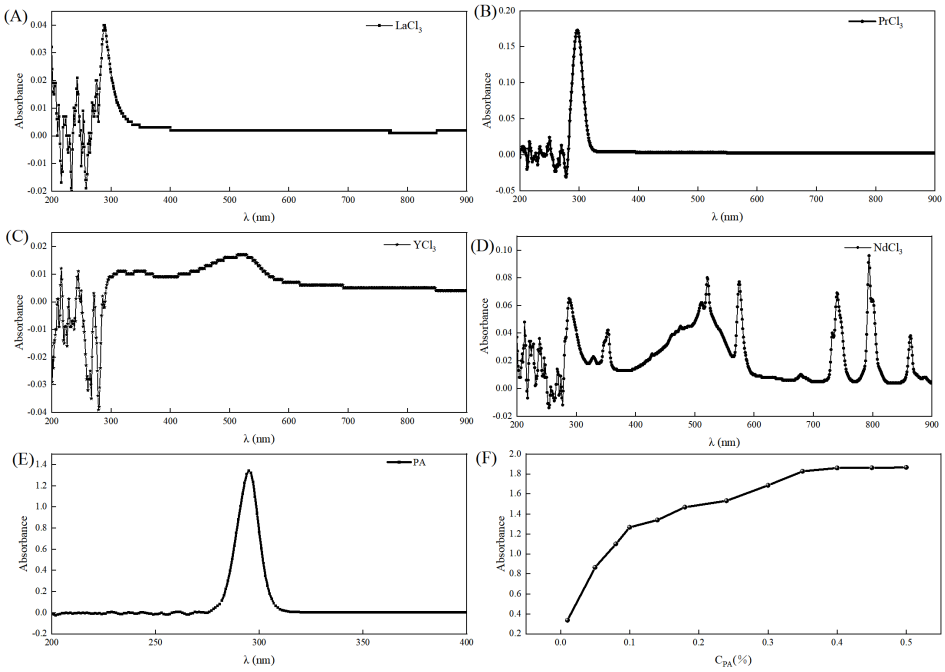

Fig. 9. Absorption spectra of $RECl_3$ and PA, and the relationship between PA concentration and absorbance. (A) $LaCl_3$; (B) $PrCl_3$; (C) YCl_3; (D) $NdCl_3$; (E) PA; (F) Relationship between PA concentration and absorbance

3.3.4. Determination of the RE^{3+} complexation coefficient with PA

The ligand excess method was employed to determine the coordination numbers of the complexes formed between RE^{3+} ions and the ligands (Gu et al., 2012). In this approach, a 0.01 mol/L RE^{3+} was first mixed with PA solutions at concentrations ranging from 0.01 to 0.05 mol/L, A series of mixed solutions was prepared with molar ratios of PA to RE^{3+} ranging from 1:2 to 5:1. The absorbance spectra of the La^{3+}, Pr^{3+}, Y^{3+} and Nd^{3+} with PA complex systems are shown in Fig. 10(A)-(D), respectively. The UV-Vis spectral features of PA in RE^{3+} solutions differed markedly from those of the individual RE^{3+} solutions. With increasing concentrations of PA, the UV-Vis absorption peaks exhibited a clear redshift accompanied by a gradual increase in absorbance intensity. This behavior can be attributed to changes

in electron cloud distribution resulting from the coordination of carboxylate oxygen atoms with RE^{3+} ions (Meng et al., 2023). When the [$RECl_3$]:[PA] ratio reached 1:3, the change in absorbance of the complexes became negligible, indicating that complex formation had essentially reached equilibrium (Meyer, 2018). Moreover, the absorption peaks of complexes formed with different RE^{3+} ions showed minimal variation, suggesting a high degree of structural similarity. This similarity likely arises from comparable coordination environments and spatial configurations, leading to nearly identical UV absorption characteristics.

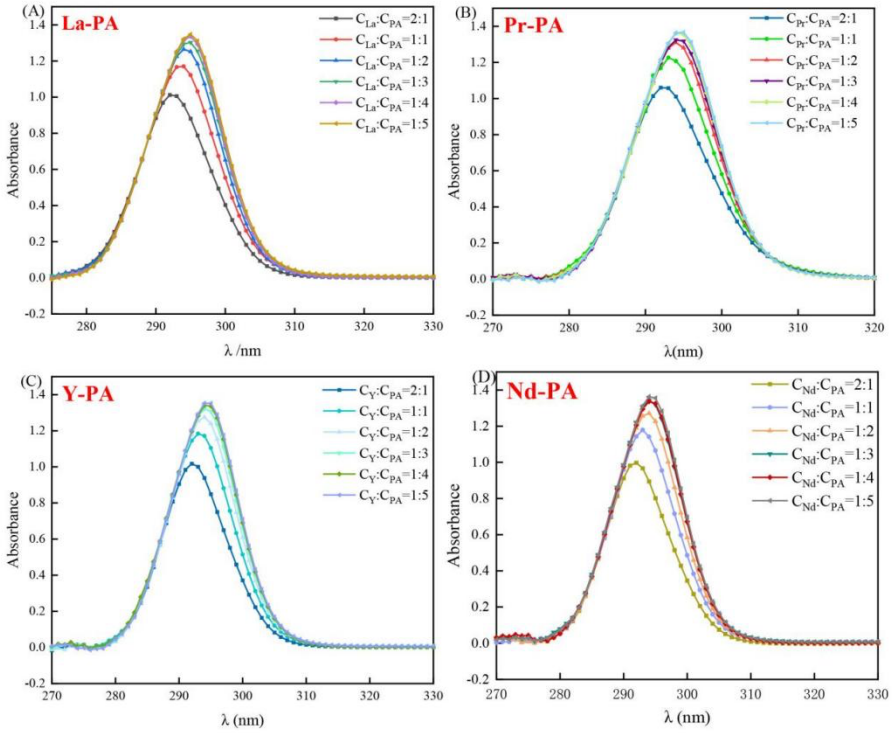

Fig. 10. Absorbance spectra of the La^{3+}(A), Pr^{3+}(B), Y^{3+} (C)and Nd^{3+} (D) with PA complex systems

The absorbance at 295 nm was plotted as a function of the molar ratio of PA to RE. Molar ratio curves of La^{3+}, Pr^{3+}, Y^{3+} and Nd^{3+} with PA complexation are shown in Fig. 11(A)-(D), respectively. The complexation coefficient was subsequently determined using the molar ratio method. The C_Y/C_M values of the aqueous RE-PA solutions fall within the range of 1.0-2.0. Specifically, the coordination number n was 1.90 for the $LaCl_3$-PA system, 1.67 for $PrCl_3$-PA, 1.38 for YCl_3-PA, and 1.78 for $NdCl_3$-PA. These results indicate that both 1:1 and 1:2 RE-PA complexes were formed in the $RECl_3$-PA aqueous solutions under the studied conditions. PA contains two carboxylate groups capable of releasing H^+ into solution. As a complexing agent, PA coordinates with RE^{3+} ions to form soluble complexes, thereby reducing the concentration of free RE^{3+} ions in the solution and promoting the transfer of adsorbed rare earth ions from the solid phase to the liquid phase (Zhao et al., 2025). The resulting RE-PA complexes migrate downward under gravity, reducing the concentration of free RE^{3+} in solution, shifting the dissolution equilibrium, and promoting further desorption of RE-bearing minerals. Consequently, the leaching efficiency is enhanced through the combined effects of acidification and complexation.

3.4. Quantum chemical calculations

3.4.1. Electron density distribution characteristic of RE^{3+} and PA

The electrostatic potential distribution of different RE^{3+} ions (La^{3+}, Pr^{3+}, $Y^{3+}$and Nd^{3+}) and PA^- are presented in Fig.12(A)-(E), respectively. Red and blue regions represent positive and negative electrostatic potentials, respectively (Zhang et al., 2017). Owing to its polar carboxyl groups, PA^- exhibits both positive and negative potential regions. Areas with lower electron density, such as hydrogen atoms and parts of the benzene ring, display relatively higher positive potentials, whereas the conjugated

benzene ring forms a moderately positive region. In contrast, the carboxyl groups, due to their electron-withdrawing effect, generate localized negative potentials, with the carboxylate moieties exhibiting particularly pronounced negative electrostatic potentials. These features enhance electron-donating ability and promote the formation of active sites (Kong et al., 2022), thereby facilitating complexation with RE^{3+} ions. All four RE^{3+} ions exhibit positive electrostatic potentials, with the magnitude following the order $Y^{3+} > Nd^{3+} > Pr^{3+} > La^{3+}$. These differences can be attributed to variations in their valence electron configurations (4f/5d orbitals) and modulation of electron density by the number of outer-shell electrons.

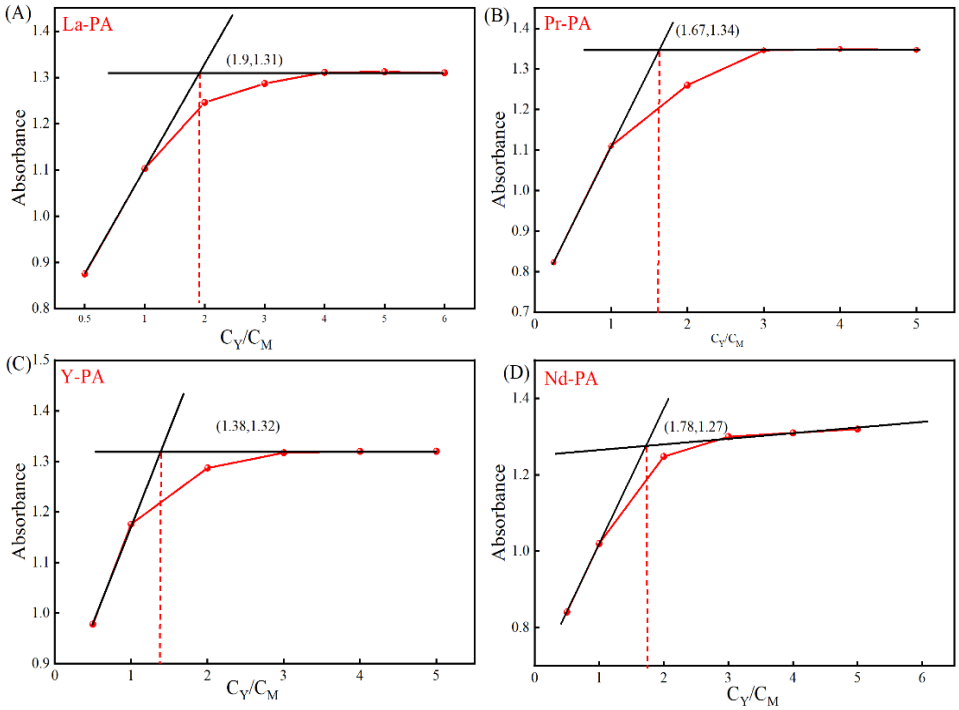

Fig. 11. Molar ratio curves of La^{3+}(A), Pr^{3+}(B), Y^{3+} (C)and Nd^{3+}(D) with PA complexation

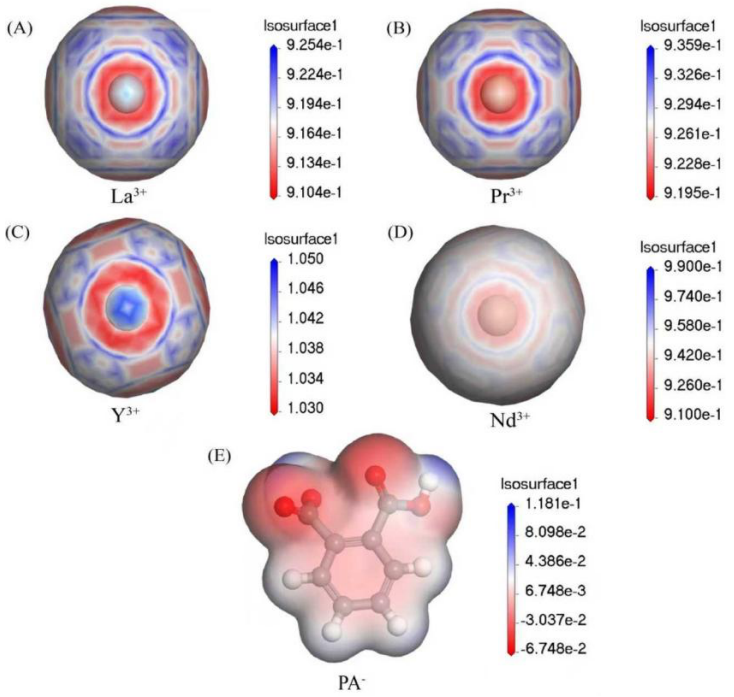

Fig. 12. Electron density calculations of different molecules

3.4.2 Calculation of the binding energy between PA^- and RE^{3+}

Based on the optimized configurations, the binding energies for the respective reactions were calculated. As shown in Fig.13, the binding energies of PA^- with La^{3+}, Pr^{3+}, Y^{3+}, and Nd^{3+} are all negative, indicating that the reactions between PA^- and the four RE ions are exothermic and yield stable complexes. Moreover, a more negative binding energy implies greater energy release and higher stability of the complex (Chen et al., 2022). The binding strength between PA^- and RE^{3+} follows the order Y^{3+}> Pr^{3+}>Nd^{3+}> La^{3+}, which is inversely proportional to the measured RE–O bond lengths. Rare earth ions with smaller ionic radii and shorter bond lengths generally exhibit stronger electrostatic attraction toward ligands. These computational results are consistent with the electrostatic potential distributions of the RE^{3+} ions, indicating that PA^- interacts more strongly with ions possessing higher charge density (Grimes and Nash, 2014). In aqueous solution, the carboxyl groups of PA ionize by releasing protons, generating negatively charged oxygen sites that can coordinate with electron-deficient RE^{3+} ions. The resulting interactions lead to the formation of stable RE carboxylate complexes (Hovey et al., 2022).

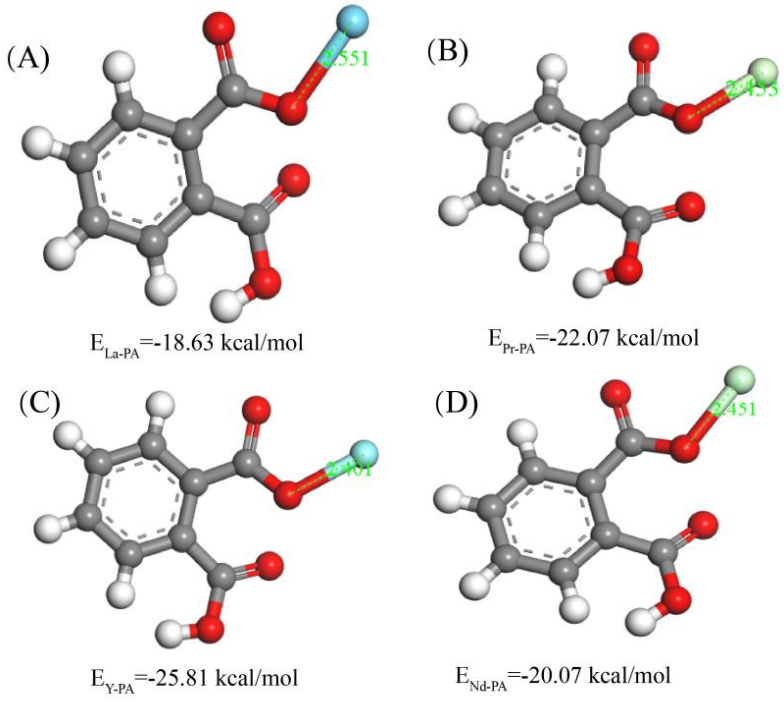

Fig. 13. Reaction binding energy between RE^{3+} and PA^- complex

4. Conclusions

This study investigates the ionic RE ores leaching behavior under a $MgSO_4$-PA composite leaching system. Optimal performance was achieved at a 0.15% PA solution, resulting in the highest RE recovery 12.5% higher than that obtained with $MgSO_4$ alone. Spectrophotometric analysis was used to investigate the interaction mechanism between PA and RE. The results indicated that in $LaCl_3$-PA solutions, n = 1.90; in $PrCl_3$-PA solutions, n = 1.67; in YCl_3-PA solutions, n = 1.38; and in $NdCl_3$-PA solutions, n = 1.78. This indicates that under these conditions, both 1:1 and 1:2 types of RE-PA complexes were simultaneously formed in the $RECl_3$-PA aqueous solution. In such low-coordination structures, the strength of the bonds formed between the central metal ion and the coordinating atoms contributes notably to the overall binding energy. The RE–O bond lengths follow the order La–O > Pr–O > Nd–O > Y–O, where shorter bond lengths correspond to stronger bonding interactions. Molecular dynamics simulation results showed that the binding energies between the four main RE^{3+} (La^{3+}, Pr^{3+}, Nd^{3+}, and Y^{3+}) ions and PA^- were all negative, indicating that the reaction between RE^{3+} and PA^- is exothermic. A larger-magnitude negative binding energy corresponds to a more stable complex. The order of binding energy magnitude for the four elements reacting with PA is Y^{3+} > Pr^{3+} > Nd^{3+} > La^{3+}. The calculation results are consistent with the electrostatic potential RE^{3+} distribution, indicating that PA^- interacts more

strongly with RE^{3+} ions that possess higher charge densities. The carboxyl groups in PA release hydrogen ions in solution, while the oxygen atoms form negatively charged sites that can complex with the electron-deficient RE^{3+} ions. This interaction facilitates the desorption of rare earth ions from the surface of clay minerals, thereby enhancing the leaching efficiency of rare earths.

Acknowledgments

All sources of funding for the study were supported by the National Natural Science Foundation of China (No.92475206, No.92462303, and No.52204280). and Open Foundation of State Key Laboratory of Mineral Processing (No. BGRIMM-KJSKL-2025-16).

References

CHANG S., LI M., GAO K., ZHANG D., DUAN H., MA L., RUAN Z., 2022. *Mechanism of phthalic acid collector in flotation separation of fluorite and rare earth*. Journal of Rare Earths, 40, 118–126.

CHEN J., QIU J., HUANG L., CHEN X., YANG Y., XIAO Y., 2022. *Coordination–reduction leaching process of ion-adsorption type RE ore with ascorbic acid*. Journal of Rare Earths, 41, 1225–1233.

DENG X., YU D., XU Y., HONG X., DONG W., CHI R., ZHANG Z., 2024. *Leaching process assisted by cetyltrimethylammonium chloride for weathered crust elution-deposited rare earth ores: leaching behavior, kinetic analysis and interfacial regulation*. Colloids and Surfaces A, 703, 135192.

DEVANGAD P., TAMBOLI M., SHAMEEM K., NAYAK R., PATIL A., UNNIKRISHNAN V., KUMAR G., 2018. *Spectroscopic identification of rare earth elements in phosphate glass*. Laser Physics, 28, 015702.

DUTTA T., KIM K., UCHIMIYA M., KWON E., JEON B., DEEP A., YUN S., 2016. *Global demand for rare earth resources and strategies for green mining*. Environmental Research, 150, 182–190.

FENG J., ZHOU F., CHI R., LIU X., XU Y., LIU Q., 2018. *Effect of a novel compound on leaching process of weathered crust elution-deposited rare earth ore*. Minerals Engineering, 129, 63–70.

GAO L., WANG Y., OYANG J., GAO Y., LIU J., WANG R., LI J., 2023. *Removal of aluminum from synthetic rare earth leach solution by selective complexation and turbidity point extraction*. Minerals, 13, 1462.

GRIMES T., NASH K., 2014. *Acid dissociation constants and rare earth stability constants for DTPA*. Journal of Solution Chemistry, 43, 298–313.

GU H., XIAO S., XIAO H., XIAO Y., LI A., XIAO L., QIANG G., 2012. *Synthesis, characterization, and thermodynamic properties of the rare earth coordination complex [Sm(C6H4NO2)2·C9H6NO]*. Industrial & Engineering Chemistry Research, 51, 3250–3257.

GUO Q., LI Z., PAN J., LI B., ZHAO L., LIU D., WANG C., 2023. *Leaching mechanism of aluminum during column leaching of ion-adsorption rare earth ore using MgSO4*. Minerals, 13, 401.

GUO X., SUN H., SUN X., 2016. *Structure, bonding, and electronic properties of four rare earth complexes with a phenoxyacetic acid ligand: X-ray diffraction and DFT studies*. Industrial & Engineering Chemistry Research, 55, 6716–6722.

HAN A., LI Z., ZHENG X., LIU D., ZHAO L., FENG Z., HUANG X., 2025. *Readsorption of rare earths and aluminum during column leaching of ion-adsorption rare earth ore using magnesium sulfate in the presence of lean ore layer*. Journal of Rare Earths.

HOSHINO M., MATSUSHITA M., SAMMA M., ASANO M., YAMAGUCHI T., FUJITA Y., 2011. *Spectrophotometric determination of cobalt(II) and cyanocobalamin with vanillilfluorone and its applications*. Chemical and Pharmaceutical Bulletin, 59, 721–724.

HOVEY J., DITTRICH T., ALLEN M., 2022. *Coordination chemistry of surface-associated ligands for solid-liquid adsorption of rare-earth elements*. Journal of Rare Earths, 41, 1–18.

KONG L., ZHANG J., WANG Y., YAN Q., XU J., QUAN X., ZHENG C., 2022. *Bowknot-like Zr/La bimetallic organic frameworks for enhanced arsenate and phosphate removal: Combined experimental and DFT studies*. Journal of Colloid and Interface Science, 614, 47–57.

LAI F., GAO G., LI H., XIAO Y., YANG R., LI K., 2018. *Compound leaching of RE from the ion-adsorption type rare earth ore with MgSO4 and ascorbic acid*. Hydrometallurgy, 179, 25–35.

LI M., ZHANG X., LIU Z., HU Y., WANG M., LIU J., YANG J., 2013. *Kinetics of leaching fluoride from mixed rare earth concentrate with hydrochloric acid and aluminum chloride*. Hydrometallurgy, 140, 71–76.

LI Y., DONG L., LI B., LI Y., SHI P., YANG H., ZHOU Z., 2025. *Selective recovery of neodymium from NdFeB wastes by chlorinated roasting and citric acid leaching*. Chemical Engineering Science, 307, 121351.

LIU D., YAN W., ZHANG Z., CHI R., 2023. *Effect of particle gradation on pore structure and seepage law of solution in weathered crust elution-deposited rare earth ores*. International Journal of Mining Science and Technology, 33, 1261–1272.

LIU W., YOON R., 2025. *Leaching kinetics of rare earth elements from NaOH-treated monazite by ammonium sulfate and carboxylate ligands*. Minerals Engineering, 233, 109654.

LIU Z., LV X., LIU E., SHEN K., ZHOU W., SUN H., 2025. *Quantum chemical calculation of the interaction between unsymmetrical dimethylhydrazine and water molecules*. Chemical Physics Letters, 870, 142058.

LUO X., ZHANG Y., ZHOU H., HE K., LUO C., LIU Z., TANG X., 2022. *Review on the development and utilization of ionic rare earth ore*. Minerals, 12, 554.

MABROUK M., HAMMAD S., ABDELAZIZ M., 2018. *Ligand exchange method for determination of mole ratios of relatively weak metal complexes: a comparative study*. BMC Chemistry, 12, 142.

MENG X., ZHAO H., ZHAO Y., SHEN L., GU G., QIU G., 2023. *Effective recovery of rare earth from (bio)leaching solution through precipitation of rare earth-citrate complex*. Water Research, 233, 119752.

MEYER G., 2018. *Small cause-great effect: What the 4fn+15d0→4fn5d1 configuration crossover does to the chemistry of divalent rare-earth halides and coordination compounds*. Journal of Solid State Chemistry, 270, 324–334.

PARHI P., PARK K., 2013. *A kinetic study on hydrochloric acid leaching of nickel from Ni-Al2O3 spent catalyst*. Journal of Industrial and Engineering Chemistry, 19, 589–594.

SHUAI Z., ZHU Y., GAO P., HAN Y., 2024. *Rare earth elements resources and beneficiation: a review*. Minerals Engineering, 218, 109011.

TIAN J., YIN J., CHEN K., RAO G., CHI R., 2011. *Extraction of rare earths from the leach liquor of the weathered crust elution-deposited rare earth ore with non-precipitation*. International Journal of Mineral Processing, 98, 125–131.

TRAORE M., HE Y., WANG Y., GONG A., QIU L., BAI Y., LIU Y., ZHANG M., CHEN Y., HUANG X., 2023. *Research progress on the content and distribution of rare earth elements in rivers and lakes in China*. Marine Pollution Bulletin, 191, 114916.

WANG H., LI L., HU J., FANG Y., LIU Y., WANG J., CHI R., XIAO C., 2025. *Enhanced leaching process of ion-adsorbed rare earth ores with itaconic acid and MgSO4 compound leaching agent*. Chemical Engineering and Processing, 208, 110137.

WANG Y., GAO F., SUN B., CHEN W., NIE Z., 2025. *Life cycle assessment for RE production from ion-adsorption deposits: A comparative study of MgSO4 and (NH4)2SO4 leaching techniques*. Journal of Environmental Management, 385, 125627.

WU J., ZHANG D., YANG T., XIA D., 2023. *Selective recovery of low-concentration light rare earth ions from high-concentration (NH4)2SO4 system by coordination ability*. Journal of Sustainable Metallurgy.

XIAO Y., CHEN Y., FENG Z., HUANG X., HUANG L., LONG Z., CUI D., 2015. *Leaching characteristics of ion-adsorption type rare earths ore with MgSO4*. Transactions of Nonferrous Metals Society of China, 25, 3784–3790.

YAN H., LIANG T., LIU Q., QIU T., AI G., 2018. *Compound leaching behavior and regularity of ionic rare earth ore*. Powder Technology, 333, 106–114.

YANG H., SHA A., HE Z., WU C., XU Y., HU J., CHI R., 2024. *Leaching kinetics and permeability of polyethyleneimine added (NH4)2SO4 on weathered crust elution-deposited rare earth ores*. Journal of Rare Earths, 42, 1610–1619.

YANG L., LI C., WANG D., LI F., LIU Y., ZHOU X., LI Y., 2019. *Leaching ion adsorption rare earth by aluminum sulfate for increasing efficiency and lowering the environmental impact*. Journal of Rare Earths, 37, 429–436.

YU B., HU Z., ZHOU F., FENG J., CHI R., 2019. *Lanthanum (III) and yttrium (III) adsorption on montmorillonite: the role of aluminum ion in solution and minerals*. Minereral Processing and Extractive Metallurgy Review, 41, 107–116.

YUN R., CHEN H., SHI J., YAN N., WANG Y., CHEN T., WANG W., 2025. *A novel extraction process for efficient recovery of rare earth elements from the leaching liquor of ion-adsorption type rare earth ore using unsaponified N,N-di(2-ethylhexyl)-diglycolamic acid*. Chemical Engineering Science, 302, 120820.

ZHANG H., YUAN S., SUN J., LIU J., LI H., DU N., HOU W., 2017. *Molecular dynamics simulation of sodium dodecylsulfate (SDS) bilayers*. Journal of Colloid and Interface Science, 506, 227–235.

ZHAO M., ZHANG H., HAN H., JIANG X., YANG Y., LI T., 2025. *Differential leaching mechanisms and ecological impact of organic acids on ion-adsorption type rare earth ores*. Separation and Purification Technology, 362, 131701.